



Molecular dynamics study of CH₄ storage and flow characteristics in non-homogeneous pore structures of coals with different morphologies

Chao Xu ^{a,b}, Wenjing Wang ^a, Kai Wang ^{a,b,*}, Lin Guo ^a, Tong Yang ^a, Yongwang Yuan ^a, Yuanyuan Hu ^a

^a School of Emergency Management and Safety Engineering, China University of Mining and Technology (Beijing), Beijing, 100083, China

^b Beijing Key Laboratory for Precise Mining of Intergrown Energy and Resources, China University of Mining and Technology (Beijing), Beijing, 100083, China

ARTICLE INFO

Keywords:

Coal
CH₄
Adsorption-desorption-diffusive
Pore morphology
Molecular simulation

ABSTRACTS

The nanoscale pore structure in coals is highly non-homogeneous and morphologically diverse, which affects the enrichment pattern and reserve prediction of coalbed methane (CBM). Due to the difficulty characterising the pore morphology of coals and the high observation requirements, there are fewer studies on the relationship between pore morphology and CBM storage and flow characteristics. Thus, non-homogeneous pore models with different shapes and degrees of openness were constructed in this paper. The simulation method of the CH₄ adsorption-desorption-diffusion process in the pore models was proposed using the grand canonical Monte Carlo (GCMC) and molecular dynamics (MD) methods. The changes in the CH₄ adsorption-desorption capacity, occurrence characteristics, diffusion laws, and energy distribution with the pore morphology were analysed. The microscopic influence mechanism of coal pore morphology on CH₄ adsorption-desorption-diffusion characteristics was revealed. The results indicated that the number of adsorbed-layer CH₄ in slit pores was 1.5–3 times higher than that in other pores. The presence of adsorbed-layer CH₄ made the effective flow distance of free-layer CH₄ only 29.20%–74.50% of the actual pore diameter. In the passing pores, the pore morphology had less effect on the diffusion movement of CH₄. In the dead-end pores, the self-structured features of cone and ink bottle pores promoted and inhibited the diffusive behaviours of CH₄ desorption, respectively. The CH₄ desorption usually released 97% of the total energy in 5 ps. The values of the released energy were in the order of slit pore > cylinder pore > ink bottle pore > cone pore. The research results will provide theoretical references for accurately predicting CBM production and improving CBM mining efficiency.

1. Introduction

Coalbed methane (CBM) is an unconventional natural gas with three essential attributes of energy, safety and environmental protection, and the output efficiency and storage law of CBM is related to the healthy development of the natural gas industry and the realisation of the national carbon neutrality goal [1]. However, the primary storage space of CBM is the nanoscale pore structure in coals, and the complexity and diversity of these pore structures have exacerbated the difficulty of researching the storage and transport characteristics of CBM and the mechanism of coal and gas protrusion [2,3]. Therefore, an in-depth investigation of the influence of coal bed pore morphology on the adsorption-desorption-diffusion law of CBM is crucial to enhance the efficiency of CBM output and reduce the occurrence of coal and gas protrusion accidents [4,5].

Recently, domestic and foreign researchers have conducted various studies on the pore morphology of coals by using scanning imaging techniques (atomic force scanning electron microscopy, focused ion beam scanning electron microscopy, field emission scanning electron microscopy, nano-CT scanning, etc.) [6], fluid intrusion techniques (low-temperature N₂ or CO₂ adsorption, and mercury intrusion porosimetry) [7], and numerical simulation techniques [8,9]. Researchers have discovered pore structures in coals containing different shapes (slit, cylinder, wedge, ink bottle, cone, triangular, and square pores) [10,11] and different degrees of openness (passing, dead-end, and closed pores) [12,13] by using scanning imaging techniques and fluid intrusion techniques. However, the fluid intrusion technique cannot achieve quantitative characterisation of different morphological pores and cannot directly observe the different morphological features of pores in coals. Although the scanning imaging technique can visualise the pore morphology in coals, the method cannot simultaneously meet the

* Corresponding author.

E-mail address: k.wang@cumtb.edu.cn (K. Wang).

Nomenclature

CBM	Coalbed methane
MS	Materials studio
PV	Pore volume
SSA	Specific surface area
PSD	Pore size distribution
C-pore	Closed pore
D-pore	Dead end pore
P-pore	Passing pore
GCMC	Giant Canonical Monte Carlo
MD	Molecular dynamics
PED	Potential energy distribution
RDF	Radial distribution function
CN	Coordination numbers
MSD	Mean square displacement
Adsorbed-layer CH ₄	Tightly bound adsorption layer of CH ₄
Free-layer CH ₄	Free diffusion layer of CH ₄

realistic demands of affordability, quantitative characterisation, speed and non-destructiveness [14]. Therefore, numerical simulation has become an essential technical tool for studies related to the pore structure of coals [15], in which the Giant Canonical Monte Carlo (GCMC) and molecular dynamics (MD) methods are often applied by domestic and foreign researchers in studies related to exploring the relationship between the pore structure characteristics of coals and the storage and transportation of CBM [16,17], which reveal many micro-mechanisms that cannot be accurately described under experimental conditions [18]. Sidorenkov et al. [19] used molecular simulation to study the pressure-driven flow of CH₄ in cylinder, square, and triangular nanopores with different sizes and different fluid-wall interaction strengths. Shi et al. [20] investigated the laws of the driving force, pore size, temperature, and pressure effects on methane adsorption/desorption and flow in coal nanopores based on molecular dynamics. Hao et al. [21] performed a series of molecular simulations after constructing different crevice pore coal models. They found that increased pore size could promote self-diffusion and transport diffusion of CH₄. However, there are still fewer related studies that comprehensively consider the pore morphology and degree of openness of coals, and the existing research results are insufficient to accurately describe the mechanism of the influence of coal pore morphology on the storage and transport characteristics of CBM. Clarifying the relationship between coal pore morphology and the adsorption-desorption-diffusion characteristics of CBM using GCMC and MD methods is still a scientific challenge that needs to be solved in CBM development and utilisation. Therefore, the successful construction of different morphology non-homogeneous coal pore models is a crucial prerequisite for the smooth progress of the study.

For this reason, researchers often use rigid carbon atoms, graphene or carbon nanotubes, etc., as the basic configuration for constructing coal pore models [8], which are polymerised into idealised pore models with different shapes or different degrees of openness based on which subsequent numerical simulation analyses are carried out. These types of pore models usually have smooth and uniform wall surfaces. However, the pore structure of coals is strongly non-homogeneous and anisotropic on the nanoscale. There is still a large gap between the idealised pore model and the pore structure of inaccurate coals [22], which makes it difficult to accurately describe the adsorption-desorption-diffusion laws of CBM in pore models of accurate coals with the study results obtained under the idealised pore models [15].

The nanoscale pore structure in coals is highly non-homogeneous and morphologically diverse, which affects the enrichment pattern

and reserve prediction of CBM. However, due to the difficulty in characterising the pore morphology of coals and the high observation requirements, the natural morphology and gas-containing characteristics of coal pores are still poorly understood, and there are few articles on the influence of coal bed pore morphology on the storage and transport characteristics of CBM. Therefore, slit (square), cylinder, cone (wedge), ink bottle and sphere pores were constructed based on the coal macromolecule model in this paper. Different degrees of openness (closed, dead-end and passing pores) were set. Then, the CH₄ adsorption-desorption-diffusion process simulation methods in different morphology pore models were proposed based on the GCMC and MD methods. Then, the changes in the CH₄ adsorption-desorption capacity, occurrence characteristics, diffusion laws, and energy distribution with the pore morphology were analysed, revealing the influence of differences in pore morphology characteristics of coals on the storage and transportation properties of CBM from a molecular point of view. The expected research results will provide a reference for accurately predicting CBM production and promoting the development of CBM extraction technology.

2. Models and methodology

2.1. Construction and validation of the pore model

In this paper, we applied the crystal filling method [23] to complete the construction of pore structure models in Materials Studio (MS) software. The pore models' diameters (length and width) were set to 2 nm, in which the sphere diameter of the inner cavity of the ink bottle pore was 2 nm, and the cylinder diameter of the outer cavity was 1 nm. The specific modelling process was as follows:

- (1) Choose diamond crystals (Fig. 1(a)) as the basic configuration of the built-in filling material and polymerise it into the desired shape, as in Fig. 1(b).
- (2) Fix the crystals in the periodic cell (Fig. 1(c)), and then run the Packing task in the Amorphous Cell module to fill the coal macromolecule model C₁₉₆H₁₃₂O₁₀N₂ (Fig. 1(d)) [24] into the periodic cell and then cycle the process of 'filling-optimising-adjusting-filling' until the coal macromolecule occupies the remaining space of cell, as in Fig. 1(e).
- (3) Use the 'Forcite' module to optimise the geometry, annealing simulation and dynamical relaxation of the filled cell to obtain the pore model with optimal energy and structure.
- (4) Remove the filled crystals in the cell to get the final pore models; see Table 1 for more details.

In this paper, the accuracy of the constructed pore model is mainly verified by the cell density. As shown in Table 1, the density value of the pore model is between 1.50–1.57 g/cm³, which is close to the measured density value of 1.57 g/cm³ of the selected coal samples in this paper [24]. It is considered that the constructed pore model meets the density requirement of the actual coal samples and ensures the consistency of the variables except the pore morphology.

Subsequently, the 'Atom Volumes & Surfaces' tool in MS was used to construct Connolly surfaces using a spherical probe with a diameter of 0.384 nm (the kinetic diameter of the CH₄ molecule), as shown in Fig. 2, with the grey colour indicating the volume occupied by the coal macromolecular structure, and the purple surface marking the pore space, the pore volume (PV) and specific surface area (SSA) of each pore model were calculated in Table 1. Then, the pore slices were made along the XZ plane, and it was found that the constructed pore model had strong non-homogeneity and a relatively rough surface. It is once again confirmed that the pore model built in this paper is closer to the natural pore structure of the coal, and the simulation results obtained by the above pore model are reliable.

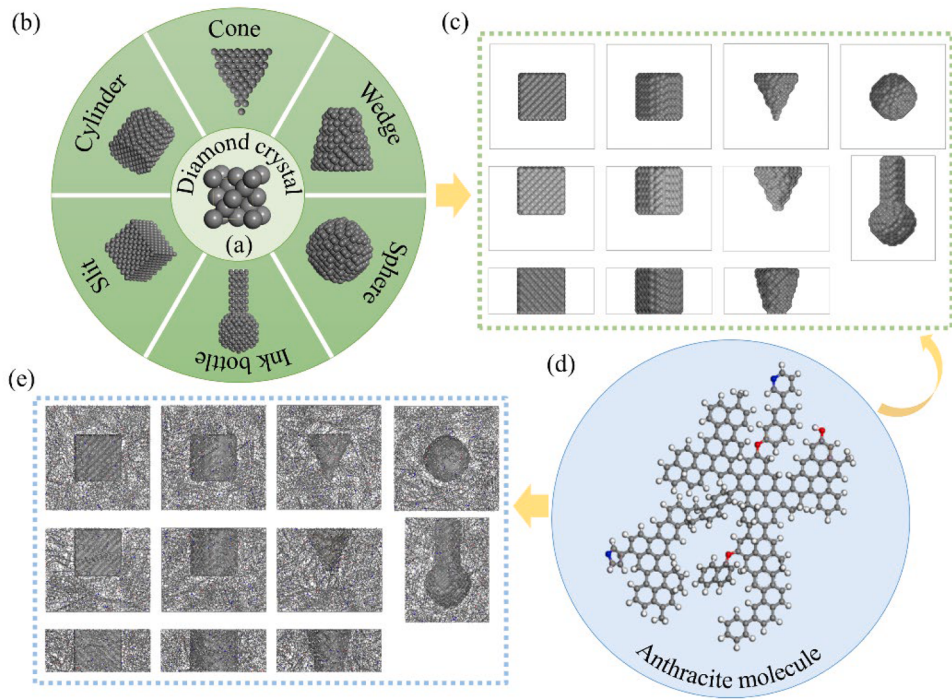


Fig. 1. Pore models construction process

Table 1
Simulation scheme and pore structure parameters

Pore model	Pore Connectivity	Pore Shape	PV (nm ³)	SSA (nm ²)	Density (g/cm ³)
S-0	Closed pore (C-pore)	Slit	14.09	52.44	1.52
Cy-0		Cylinder	8.28	28.01	1.57
Co-0		Cone	5.39	33.64	1.53
Sp-0		Sphere	7.54	33.43	1.50
S-1	Dead end pore (D-pore)	Slit	13.26	41.65	1.52
Cy-1		Cylinder	8.90	24.48	1.57
Co-1		Cone	3.59	17.05	1.50
I-1		Ink bottle	8.26	27.05	1.52
S-2	Passing pore (P-pore)	Slit	12.69	36.69	1.52
Cy-2		Cylinder	7.67	21.48	1.54
Co-2		Cone	5.59	15.99	1.56

generating time series, and computing parameter estimates and statistics. It can capture the adsorption mechanism of CBM in coal pores because the events are stochastic [25]. GCMC has been widely used to simulate the process of particle number change due to molecular adsorption on surfaces, phase transitions, and atomic nuclear reactions [26,27]. MD simulation can capture the flow characteristics of gas molecules in porous materials at the microscopic level [28], which researchers have confirmed to be applied to study gas desorption characteristics in porous materials [19,22]. Therefore, this paper applies the GCMC-MD method to simulate the CH₄ adsorption-desorption-diffusion characteristics in pore models.

As shown in Fig. 3, firstly, the isothermal adsorption of CH₄ in different pore models was simulated based on the GCMC method by applying the 'Sorption' module to obtain the equilibrium adsorption configuration with the lowest energy, which was also the initial configuration for the desorption simulation. Subsequently, a vacuum layer was inserted in the Z direction of the equilibrium adsorption configuration to simulate the gas-phase space outside the adsorption configuration. Finally, the 'Forcite' module based on the MD method was used to simulate the instantaneous desorption of gas molecules in the coal pore models and their diffusion into the gas-phase space so that the microscopic simulation was used to invert the macroscopic desorption phenomenon commonly found in practical engineering applications. The specific simulation parameters are shown in Table 2, in which the pressure change in the MS software is achieved by adjusting the fugacity, so the pressure needs to be converted to the corresponding fugacity for simulation [29].

It should be noted that the CH₄ gas inside the C-pores is formed in long-term geological evolution under actual engineering conditions. Therefore, the simulation of CH₄ adsorption in the C-pores based on the GCMC method in this paper is an inversion of the form of CH₄ storage in the C-pores, and the term 'adsorption' is used in the following to describe the CH₄ storage in the C-pores, unless otherwise specified.

2.2. Simulation methodology

GCMC methods investigate the distributional characteristics of the solution problem by setting up a stochastic process, repeatedly

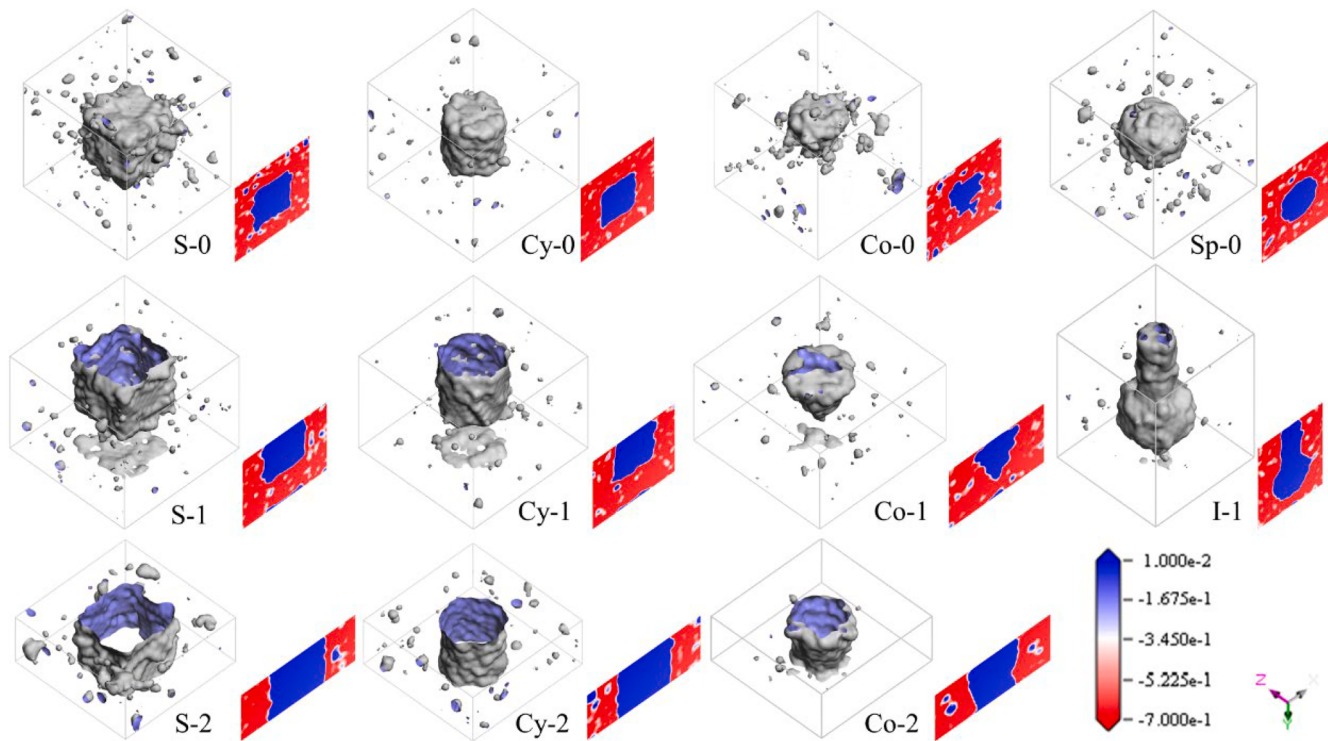


Fig. 2. Distribution of pore structure in different pore models

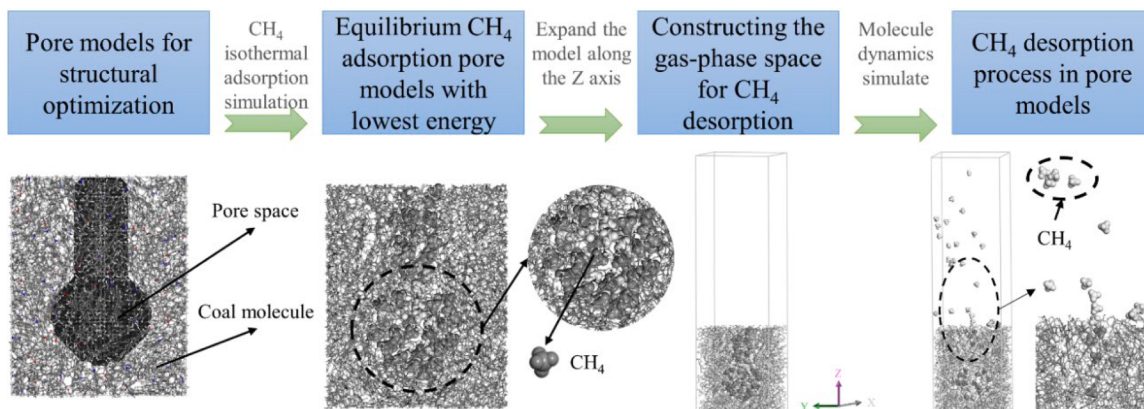


Fig. 3. Flow chart for simulation of CH_4 adsorption-desorption-diffusion in coal pores

Table 2
Parameter settings for GCMC and MD simulations

Setting	Parameter	Setting	Parameter
Method	Metropolis	Equilibration steps	1×10^6
Quality	Customized	Production steps	1×10^6
Forcefield	COMPASS II	Sample interval	25
Charges	Forcefield assigned	Ensemble	NVT
Electrostatic	Ewald & Group	Time step	1fs
van der Waals	Atom based	Fugacity steps	10
Ewald accuracy	0.001 kcal/mol	Temperature	303K
Cutoff distance	1.25 nm	Pressure	Adsorption isotherm: $0.1\sim10\text{MPa}$ Fixed pressure: 10 MPa

3. Results and discussion

3.1. Adsorption characteristics of CH_4 in different morphological pore models

3.1.1. CH_4 adsorption capacity

The unit of adsorption quantity given in the result file after GCMC simulation is $\text{N/u}\cdot\text{c}$, while the common unit of gas adsorption quantity in standard conditions is cm^3/g . Therefore, this paper applies Eq. (1) to convert the unit of adsorption quantity obtained from the simulation, and the unit of adsorption quantity is used cm^3/g in the following unless otherwise specified.

$$Q_{STP} = 22400N/M \quad (1)$$

Where N is the adsorption quantity obtained from the simulation, indicates the number of molecules adsorbed unit crystal cell, $\text{N/u}\cdot\text{c}$; Q_{STP} is the gas adsorption capacity at standard conditions, cm^3/g ; M is the

molecular mass of a single crystal cell, g/mol.

$$Q_a = Q_m K P / (1 + K P) \quad (2)$$

Where Q_m is the saturated adsorption quantity, cm^3/g ; Q_a is the absolute adsorption quantity when the gas pressure is P , cm^3/g ; K is the Langmuir equilibrium constant. Calculating the adsorbent surface coverage θ based on Eq. (3):

$$\theta = Q_a / Q_m \quad (3)$$

The Langmuir adsorption model (Eq. (2)) was applied to fit the Q_a in different morphological pore models in this paper. As seen in Fig. 4 and the fitting accuracy (R^2) in Table 3, the gas adsorption behaviour is consistent with Langmuir's law, and Q_a increases with increasing pressure. When the pressure reaches 10 MPa, the Q_a of the pore models is in the range of 11.90–66.00 cm^3/g , which in the C-pores is S-0>Cy-0>Sp-0>Co-0, in the D-pores is S-1>I-1>Cy-1>Co-1, and in the P-pores is S-2>Cy-2>Co-2. The highest value was found in the P-pores, followed by the D-pores and C-pores. Combined with the analysis of the Langmuir fitting results (Table 3), it is clear that the Q_m of slit pores is the highest under the same open conditions, which means that the adsorbed gas in the slit pores is firstly desorbed in the process of downsizing and mining of CBM production. Although the molecular weight of CH_4 adsorbed in S-2 is high, the spatial structure of its two-end openings makes it difficult to provide enough adsorption sites, which leads to lower θ and K values than those of other pores. In addition, the θ and K values of Co-0 are much higher than those of the different models since many tiny pores were formed in addition to the primary body pores during the construction of this pore model. The micropore filling with strong interaction force occurs within this part of the pores. This is also confirmed by the low fit of adsorption data to Eq. (2).

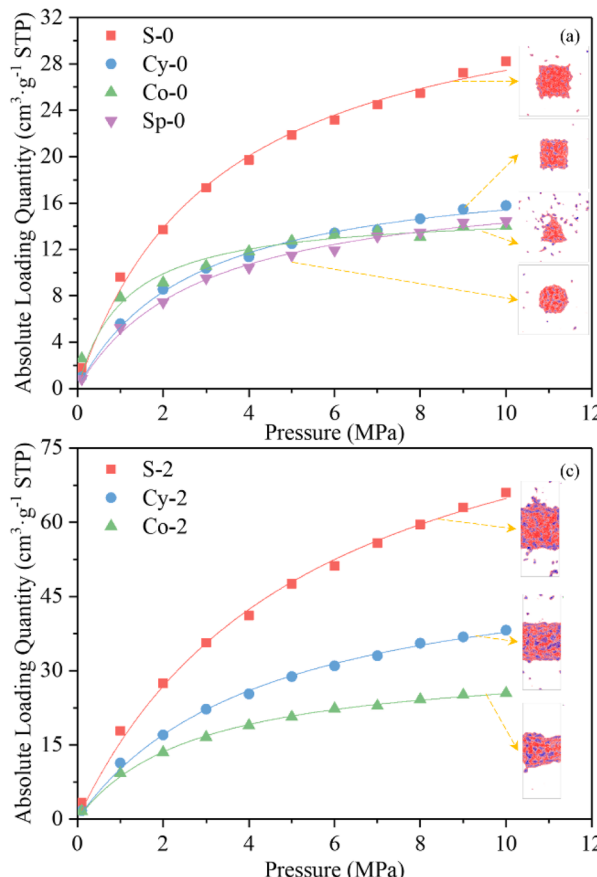


Fig. 4. Absolute CH_4 adsorption versus pressure and Langmuir nonlinear fitting curves in different pore models (a) C-pores; (b) D-pores; (c) P-pores; (d) Absolute loading quantity at 10 MPa

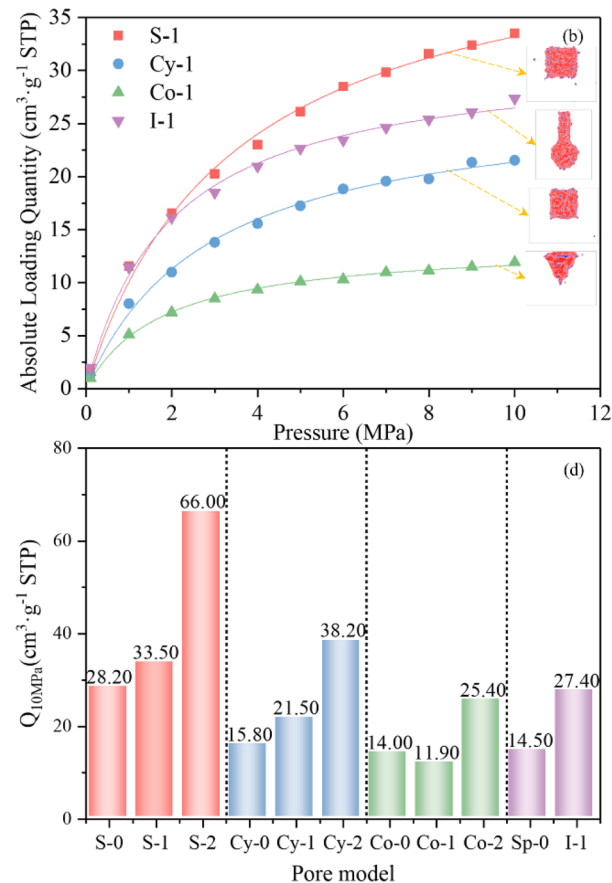
Table 3

Results of fitting the Langmuir to absolute adsorption quantity of CH_4

Pore model	Q_m (cm^3/g)	R^2	θ	K
S-0	36.35	0.995	0.78	0.31
Cy-0	19.55	0.995	0.81	0.37
Co-0	15.32	0.967	0.91	0.91
Sp-0	18.35	0.995	0.79	0.35
S-1	44.57	0.995	0.75	0.29
Cy-1	27.51	0.995	0.78	0.35
Co-1	13.72	0.997	0.87	0.55
I-1	31.65	0.996	0.86	0.51
S-2	100.07	0.996	0.66	0.18
Cy-2	54.26	0.998	0.70	0.23
Co-2	32.32	0.998	0.79	0.36

3.1.2. Energy and density distribution

Fig. 5 shows the potential energy distribution (PED) of CH_4 adsorption in different pore models. The PED is roughly arch-shaped, the low likely energy region is the dominant adsorption site, the negative value indicates the more vital interaction, and the probability peak position is the leading adsorption site [30]. As shown in Fig. 5, the PED of the pore models is about -8 to 0.25 kJ/mol , and the pore shape had less influence on the PED. Still, the region of the dominant adsorption site and the location of the probability peak of the pore changed significantly when the degree of openness was altered. In contrast, the dominant adsorption sites of C-pores and D-pores converge to the left low potential energy region, indicating that the overall adsorption strength of the two is higher than that of P-pores. The D-pores have the highest peak probability, and peak energy is close to that of the C-pores but higher than that of the P-pores, indicating that there are far more major adsorption sites in the D-pores and C-pores. The D-pores have the most difficulty



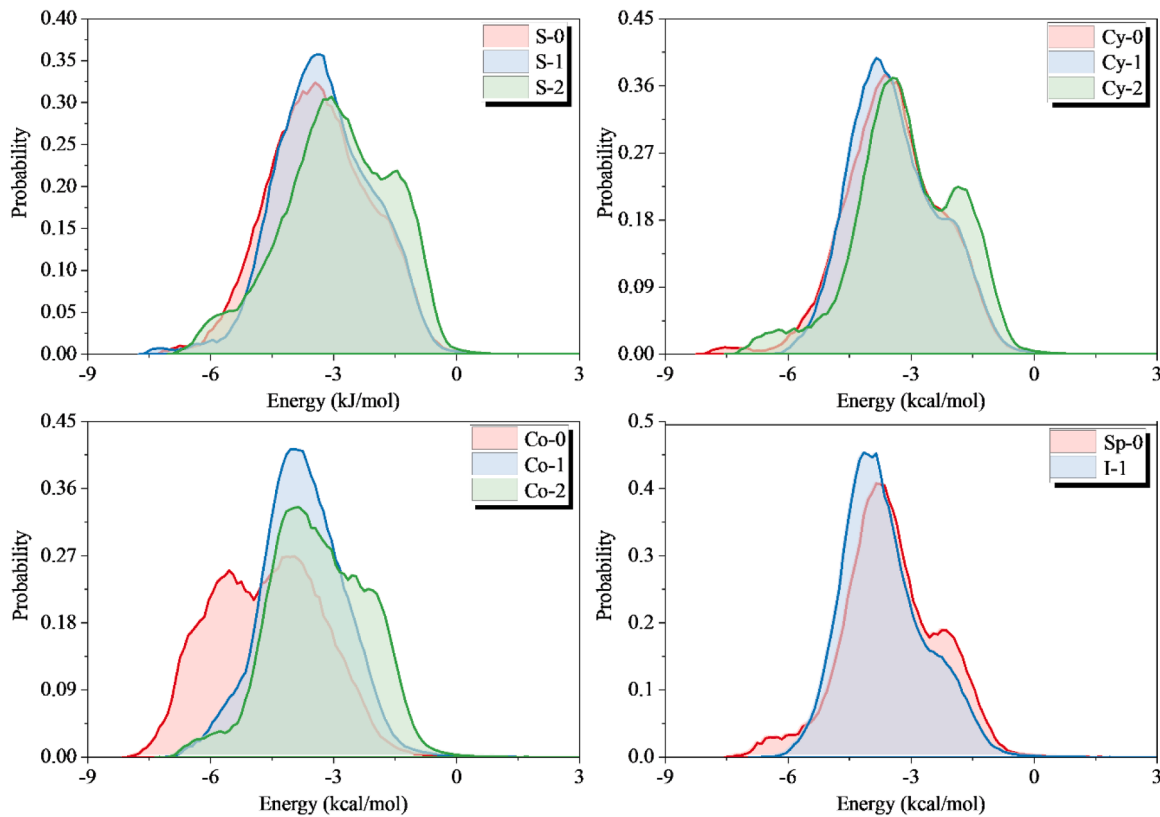


Fig. 5. PED of CH_4 adsorption in different pore models

reaching saturation during adsorption.

To better understand the influence of pore openness on the distribution of gas adsorption sites, the CH_4 density field distribution in different openness pore models under the result of varying adsorption pressures was analysed by taking the more common slit pores as an example, as shown in Fig. 6. The adsorption density field is mainly composed of low-density regions. At the 0.1–5 MPa stage, the high-density region is primarily concentrated on the surface of the pore wall. The CH_4 molecules fill the structural vacancies of coal molecules with strong adsorption potentials, the spaces between coal molecules, and the open regions on the surface of coal molecules. As the adsorption pressure increases to 10 MPa, the CH_4 molecules accumulate in the free space. Meanwhile, under the same adsorption pressure, the pore openness increased, the density of CH_4 in both the pore wall and free space decreased, and its ability to capture CH_4 gradually weakened. This is because the SSA of pores is the main factor affecting the adsorption capacity [29]. Table 1 shows that the SSA of the C-pores, D-pores and P-pores decreases sequentially, and the corresponding adsorption sites are decreasing, so there is a negative correlation between the pore openness and gas storage capacity.

3.2. CH_4 occurrence states and flow characteristics in different morphological pore models

3.2.1. CH_4 occurrence states

The absolute adsorption amount obtained from the MS software simulation refers to all CH_4 molecules inside the pore model, including the adsorbed-state CH_4 adsorbed on the pore surface and the free-state CH_4 not adsorbed in the pore space. However, the existing studies show that 85% of the CH_4 molecules in the coal are adsorbed with a micropore-filling form in the microporous structure of 0.38–1.5 nm. The remaining 15% of the adsorbed-state CH_4 and free-state CH_4 coexist in the pores above 1.5 nm, confirming the importance of adsorbed-state CH_4 in coals [31,32]. Therefore, to clarify the occurrence differences

of the adsorbed-state CH_4 in different morphological pore models, this section converts the absolute adsorption amount to the excess adsorption amount through Eq. (4) [33].

$$N_e = N_a - N_A PV_{mp} / RT \quad (4)$$

Where N_e is the excess adsorption quantity, it indicates the number of adsorbed-state CH_4 unit cells, N/u.c. . N_a is the absolute adsorption quantity obtained by simulation, N/u.c. ; N_A is the number of molecules in a mole, $6.02 \times 10^{23} \text{ mol}^{-1}$; P is the pressure of the gas, MPa; V_{mp} is measurable pore volume, $\text{cm}^3/\text{u.c.}$; R is the universal gas constant, $8.31 \text{ J}\cdot\text{mol}^{-1}\cdot\text{K}^{-1}$; T is temperature, K.

The unit conversion of N_e was completed by Eq. (1) to obtain the excess adsorption amount Q_e at the standard condition. Fig. 7 shows the Q_e of CH_4 in different morphological pore models. Except for the S-2 model, the other pore models went through the adsorption stages of rapid increase, slow increase and stabilisation of the adsorption amount. When the adsorption pressure reaches about 5 MPa, the adsorbed-state CH_4 in C-pores and D-pores tends to be saturated, while P-pores tend to be saturated at about 8 MPa. Specifically, the Q_e of CH_4 in C-pores was slit pore > cylinder pore > cone pore > sphere pore, in D-pores was slit pore > cylinder pore > ink bottle pore > cone pore and in P-pores was slit pore > cylinder pore > cone pore. Taken together, regardless of the degree of openness, the Q_e of slit pores is 1.5–3 times higher than that of other shaped pores, indicating their prominence in CH_4 storage capacity. From the basic structural parameters of the pore models (Table 1), this is because the SSA of the slit pores is much higher than that of other pores. The size of the SSA determines the amount of adsorbed CH_4 in coals, and the Q_e in D-pores, C-pores, and P-pores of the same shape shows an overall increasing trend, and it is usually P-pores > C-pores > D-pores. This is consistent with the trend of Q_m in Table 3, which indicates that the importance of slit and P-pores in CBM reservoirs should not be neglected. The Q_m mainly controls the Q_e in the pores, and the higher the Q_m is, the higher the adsorbed CH_4 content is. The Q_m can be predicted to

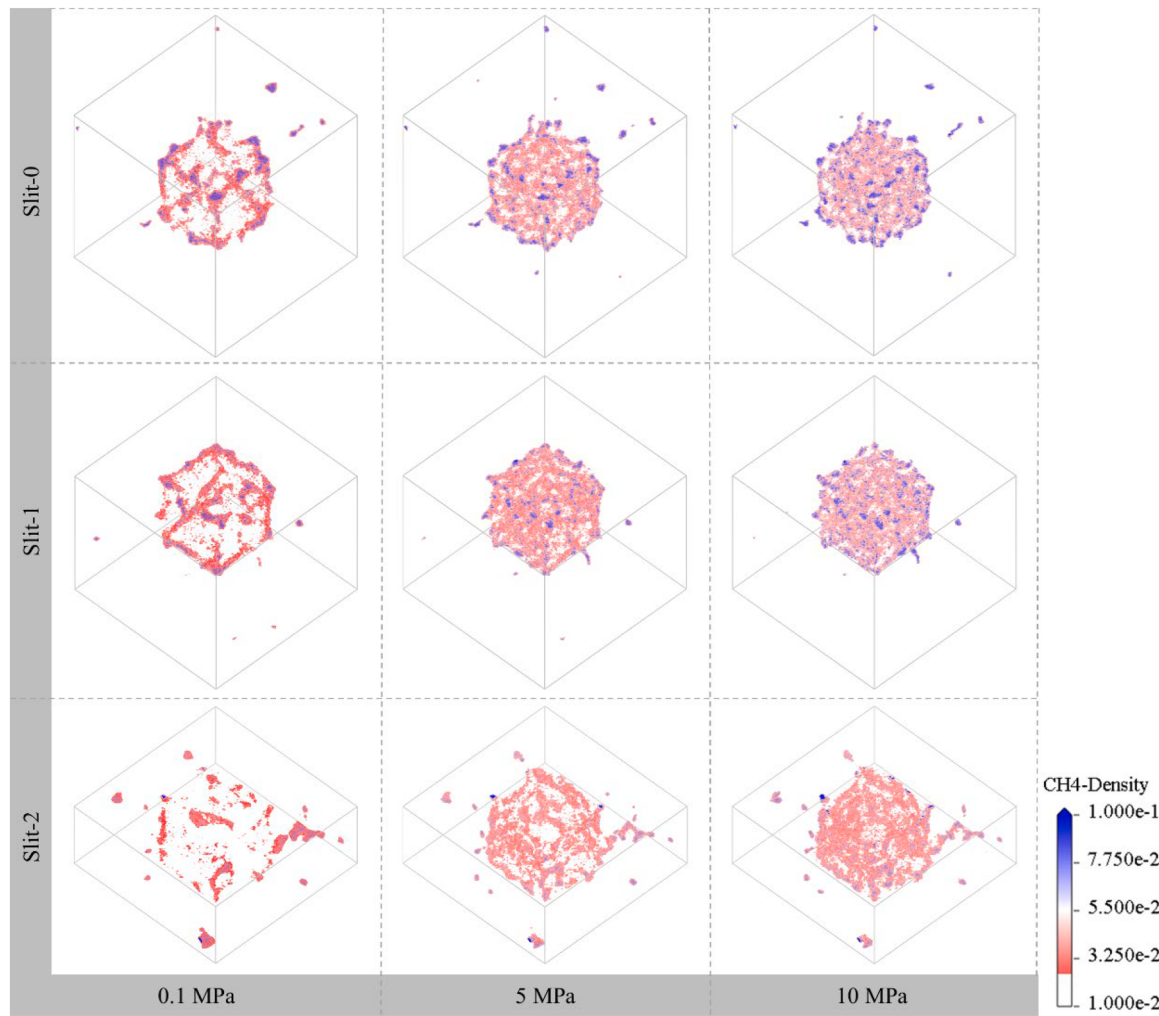


Fig. 6. CH_4 density distribution in slit pore models at different adsorption pressures

estimate the adsorbed CH_4 content of coals effectively.

The pore morphology of coals causes differences in the CH_4 adsorption capacity of coals and also leads to significant changes in the CH_4 molecular occurrence form. To achieve quantitative characterisation of gas molecules, CH_4 molecules within 0.384 nm and outside 0.384 nm near the pore wall (based on the molecular dynamics diameter of CH_4 molecules) were selected sequentially based on the law of atom group definition and defined as the tightly bound adsorption layer of CH_4 (adsorbed-layer CH_4) and the free diffusion layer of CH_4 (free-layer CH_4), respectively, as shown in Fig. 8. Then, the number of molecules in the different molecular layers was counted. The proportion to the Q_a was calculated to obtain the proportion of adsorbed-layer CH_4 to free-layer CH_4 , which was recorded as the computed value.

Eq. (4) can be applied in this paper to verify whether the selected spacing size is reasonable. This is because the quantitative relationship between N_a and N_e has been confirmed many times in existing studies by Eq. (4), which suggests that the N_e can be interpreted as the N_a of the gas in the coal sample minus the number of adsorbent gases contained in the pore space at the calculated pressure and temperature [34,35]. Based on this, this paper defines the proportion of N_e to N_a as the theoretical value n_e of the proportion of the adsorbed-layer CH_4 and $(1-n_e)$ as the theoretical value of the proportion of the free-layer CH_4 . The spacing size in the atom group definition law is considered reasonable if the error between the calculated and theoretical values is controlled within 10%.

Fig. 9 compares calculated and theoretical values of the proportion of adsorbed-layer CH_4 and free-layer CH_4 in different morphological pore

models. The proportion of adsorbed-layer CH_4 (58.81–79.29%) is higher than in the free-layer (20.71–42.19%). The low proportion of adsorbed-layer CH_4 and a high proportion of the free-layer CH_4 within the P-pores compared with the existing findings are attributed to the fact that the SSA of the P-pores is lower than that of the C-pores and D-pores, which leads to the inability of the P-pores to provide sufficient adsorption sites for CH_4 molecules. The proportions of adsorbed-layer CH_4 in different shapes of pore models are cone>ink bottle>cylinder>sphere>slit. In addition, it is found that the error between the calculated and theoretical values of similar molecular layers is controlled within 10% by comparison, indicating that the selected spacing is reasonable using the atom group definition law. Moreover, the quantitative characterisation method of the gas molecules' storage form proposed in this paper applies to different morphologies of pore models, and it can be widely used in research related to pore structure characteristics and gas storage law.

3.2.2. Flow characteristics of CH_4 molecules in different occurrence states

Even at equilibrium, gas adsorption is a dynamic process in which gas molecules either return to the free pore space to await the subsequent capture or stay along the surface. During this process, there are both intermolecular collisions and collisions of gas molecules with the pore walls, which leads to different flow patterns for adsorbed and free CH_4 . The adsorbed gas usually flows at the pore wall by surface diffusion. In contrast, the flow pattern of the free gas depends on the Knudsen number (K_n) [36,37]; see Eq. (5). To clarify the flow pattern of adsorbed state CH_4 and its impact on the flow pattern of free state CH_4 in different

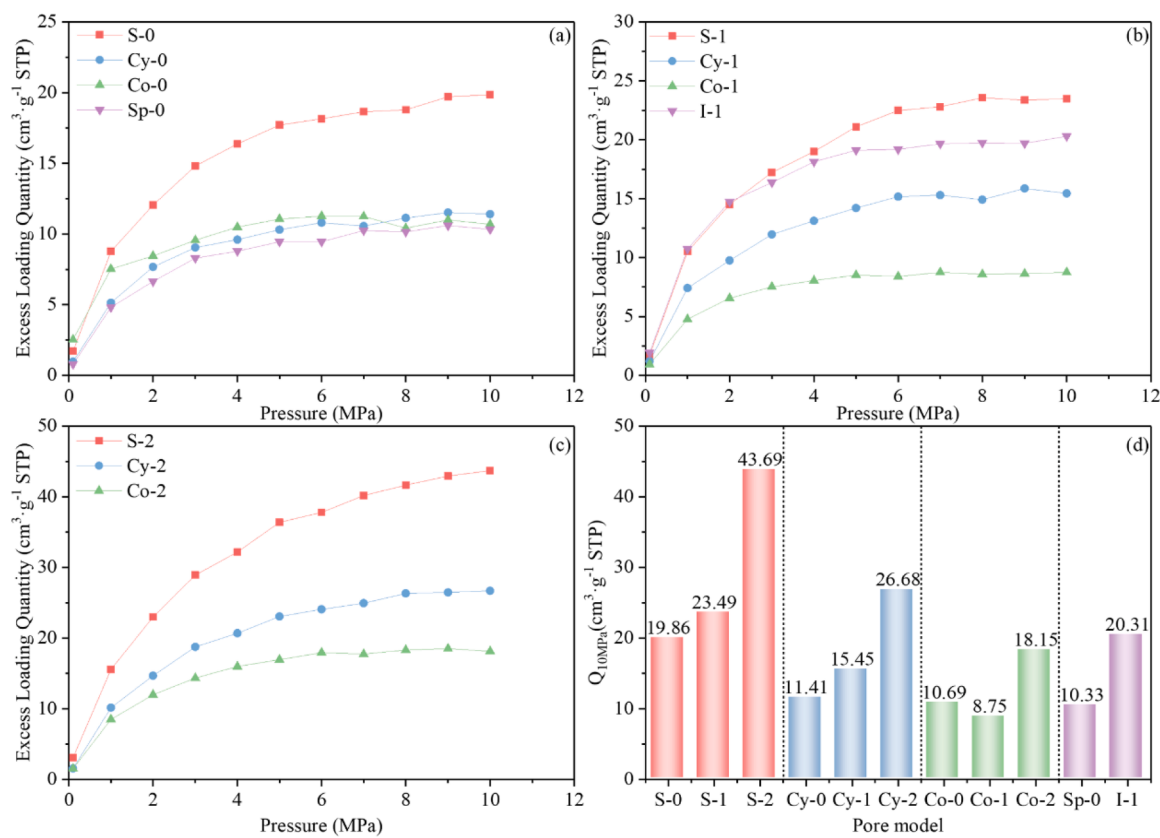


Fig. 7. Excess CH_4 adsorption versus pressure in different pore models (a) C-pores; (b) D-pores; (c) P-pores; (d) Excess loading quantity at 10 MPa

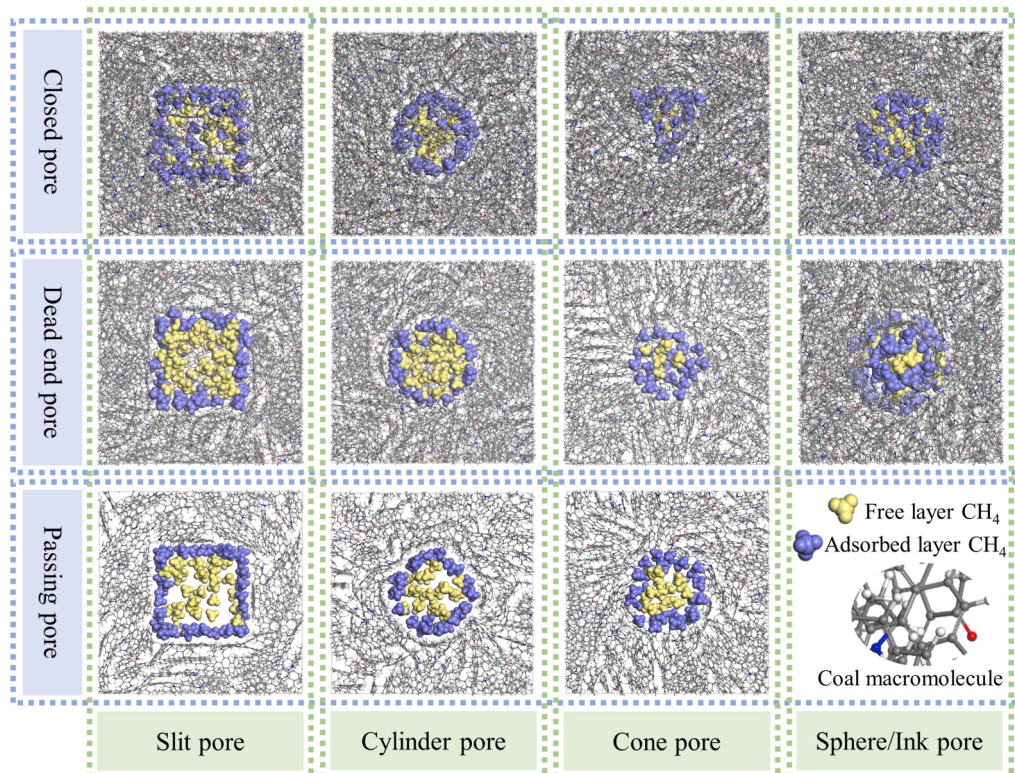


Fig. 8. CH_4 occurrence forms at adsorption equilibrium states in different pore structures

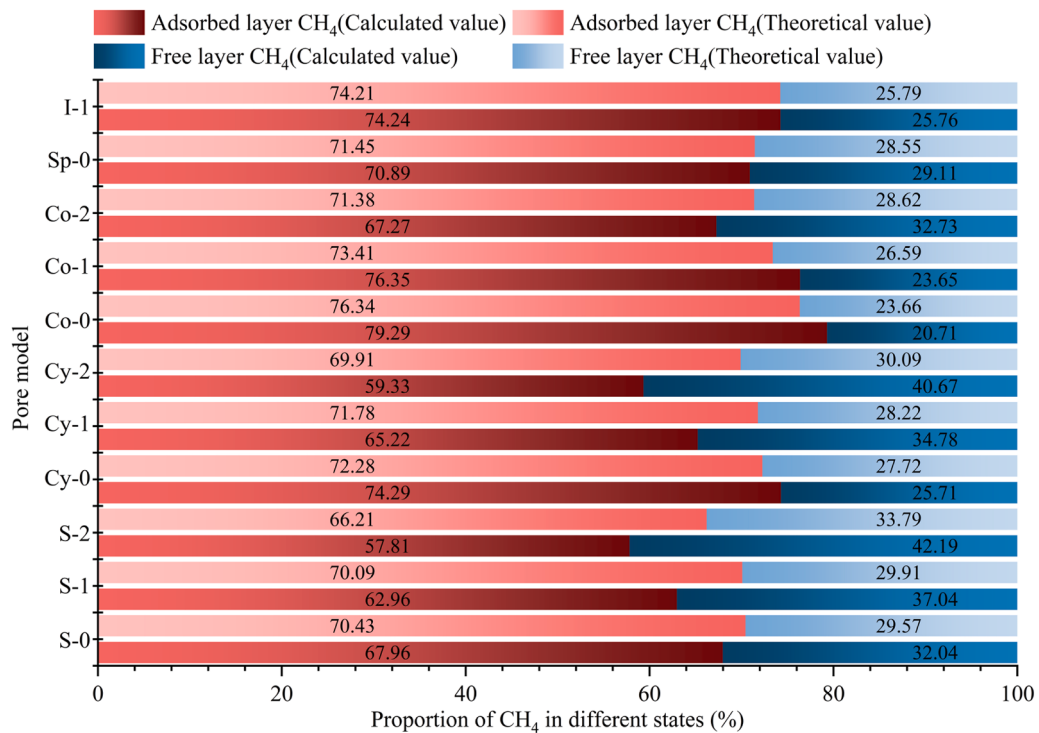


Fig. 9. Proportion of adsorbed and free layer CH₄ distribution within the pore models

morphological pore models, the free molecular adequate flow characteristic length l_{eff} in different morphological pore models is calculated in this section [38]; see Eq. (6).

$$K_n = \lambda / l_{eff} \quad (5)$$

Where λ is the average free range of the actual gas molecules, nm; l_{eff} is the adequate flow characteristic length of the free gas in the pore model of different shapes, nm.

$$l_{eff} = \begin{cases} d - 2d_m\theta \\ d_{Sphere_{eff}} + d_{cylinder_{eff}}/2 \end{cases} \quad (6)$$

Where d_m is the collision diameter of gas molecules, 0.384 nm; d represents the height of the slit pore, the diameter of the cylinder and sphere pore, the diameter of the inner tangent circle of the cone pore, nm; $d_{Sphere_{eff}}$ and $d_{cylinder_{eff}}$ are the diameters of the sphere portion and the cylinder portion in the ink bottle pore, respectively, nm; θ is the surface

coverage, %.

The l_{eff} of free-layer CH₄ in different pore models is 0.58–1.49 nm through Eq. (6), which is only 29.20–74.50% of the actual pore size (2nm), so it is necessary to consider the thickness of the adsorbed-layer CH₄. As shown in Fig. 10(a), the K_n of free-layer CH₄ flow is more significant than ten and belongs to the field of free molecular flow. In contrast, in the molecular flow regime, Knudsen diffusion is commonly used to describe the diffusivity of gases [39].

$$D_{K_n} = d\sqrt{8RT/\pi M_A}/3 \quad (7)$$

Where D_{K_n} is Knudsen diffusion coefficient, m²/s; M_A is the molar mass of the gas, g/mol.

Therefore, in this section, the D_{K_n} for free-layer CH₄ flow in different pore models are calculated by Eq. (7). The calculated results are shown in Fig. 10(b); the K_n values for free-layer CH₄ diffusion in cone pores are much higher than in other pores, while the opposite is true for D_{K_n} ,

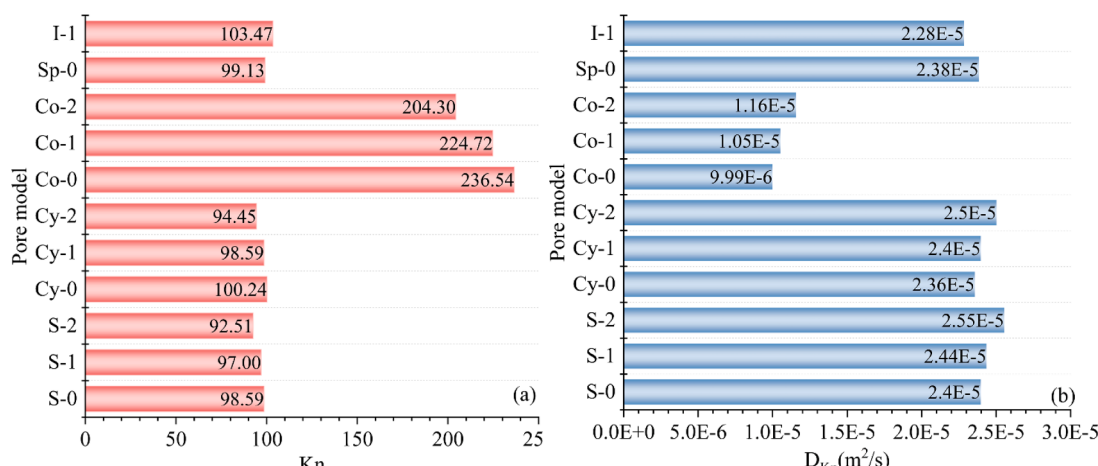


Fig. 10. Flow-diffusion parameters of free-layer CH₄ in different pore models (a) Knudsen number; (b) Knudsen diffusion coefficient

suggesting that l_{eff} in the cone pores is closer to the molecular mean free range. The stronger the discrete effects of molecules, the more complex forces between molecules cannot be ignored. In addition, except for sphere and ink bottle pores, the K_n of free-layer CH₄ in C-pores, D-pores, and P-pores of other shape pores decreases in turn and the D_K increase in demand. Cone pores have the highest proportion of adsorbed-layer CH₄, so the free-layer CH₄ diffusion flow effect within their pores is the weakest.

3.3. Characteristics of CH₄ desorption in different morphological pore models

3.3.1. CH₄ desorption capacity

In this paper, the desorption-diffusion behaviours of CH₄ molecules driven by the concentration gradient in different morphology pores of coals were simulated using MD methods. C-pores belong to a confined space, and the CH₄ gas inside cannot be desorbed and released by itself, so its desorption process is not within the scope of the study in this section.

In this section, the desorption process of CH₄ molecules in different morphology pore models is described by phase diagrams at different moments using the I-1 and S-1 models as examples, as shown in Fig. 11. In the initial desorption stage, CH₄ molecules rapidly leave the surface of the pore wall and diffuse to the low concentration region outside the pore. The CH₄ molecules inside the pore space gradually decreased with the prolongation of desorption time. However, the desorption of CH₄ from different morphological pore models varies considerably, making it difficult to estimate the amount of CH₄ remaining in the pores.

Therefore, Fig. 12 compares the adsorbed-layer and free-layer CH₄ proportion in the pore models before and after desorption. Before desorption, the proportion of adsorbed-layer CH₄ was significantly higher than that of free-layer CH₄ in all models, confirming that the adsorbed state is the primary CH₄ occurrence in coals [40]. However, due to the difference in pore morphology, the proportion of the adsorbed-layer CH₄ in the models is in the order of Co-1>I-1>Co-2>Cy-2>S-2>S-1>Cy-1, indicating that there is a non-negligible influence of pore morphology on the form of CH₄ fugacity inside it. The pore morphology needs to be considered when making CBM production predictions. When the desorption simulation is completed, except for the I-1 model, the proportion of free-layer CH₄ in the rest of the pore models is close to 100%, indicating that the CH₄ gas in the pore models is all in the free state at this time, which demonstrates the desorption and diffusion of CH₄ molecules in the pore models of different morphologies from the perspective of the micro-molecules. The

property that ink bottle pores are more challenging to desorb than other pores was shown using quantitative calculations.

3.3.2. Energy distribution

This section discusses the effect of pore morphology on system energy, pressure, and interaction strength during CH₄ desorption. Fig. 13 shows the impact of pore morphology on system energy, pressure, and interaction strength during CH₄ desorption.

Fig. 13(a) shows the variation curves of its Hamiltonian with time t during CH₄ desorption in different pore models, indicating the correlation between the sum of kinetic and potential energies of CH₄ molecules and coal macromolecules and the desorption and diffusion of CH₄ molecules on the surface of the pore model. The CH₄ molecules in different pore models reach the highest energy point within the 50 to 370ps range. The magnitude of the energy maximum is S-1>S-2>Cy-1>Cy-2>I-1>Co-2>Co-1. The energy released from desorption in slit and cylinder pores is higher than that in the ink bottles and cone pores, but the order of reaching the energy maximum is Co-1>Co-2>S-2>Cy-2>S-1>Cy-1>I-1. The cone pores are mainly affected by the PV and SSA, the initial CH₄ adsorption inside is low, which cannot provide enough power source for gas desorption, and the open pore opening in the conical space is favourable for gas desorption, so the energy increases sharply with the rapid release of CH₄ in a short period. Still, the energy released is much lower than in the other pores, and the ink bottle pores are the opposite. This is consistent with the judgment obtained in the last Section 3.1.

In addition, after the MD simulation of the model system of CH₄ and pores, the pressure versus time curve of the system was obtained in Fig. 13(b). Under the same desorption time, pressure fluctuations occur in pore models, with the overall trend decreasing, increasing, and finally stabilising. Among others, the S-1 pore model has the most significant pressure fluctuation amplitude and the highest initial desorption pressure, which explains the highest energy release in the S-1 pore model during CH₄ desorption.

Fig. 13(c) shows the curves of van der Waals forces with time during CH₄ desorption in different pore models. The interaction strength between CH₄ and coal macromolecules in D-pores (except cone pores) is higher than in P-pores, indicating that CH₄ molecules are not easily desorbed by diffusion, especially in ink bottle pores. In contrast, the diffusion coefficients of CH₄ on the pore surfaces are higher in P-pores.

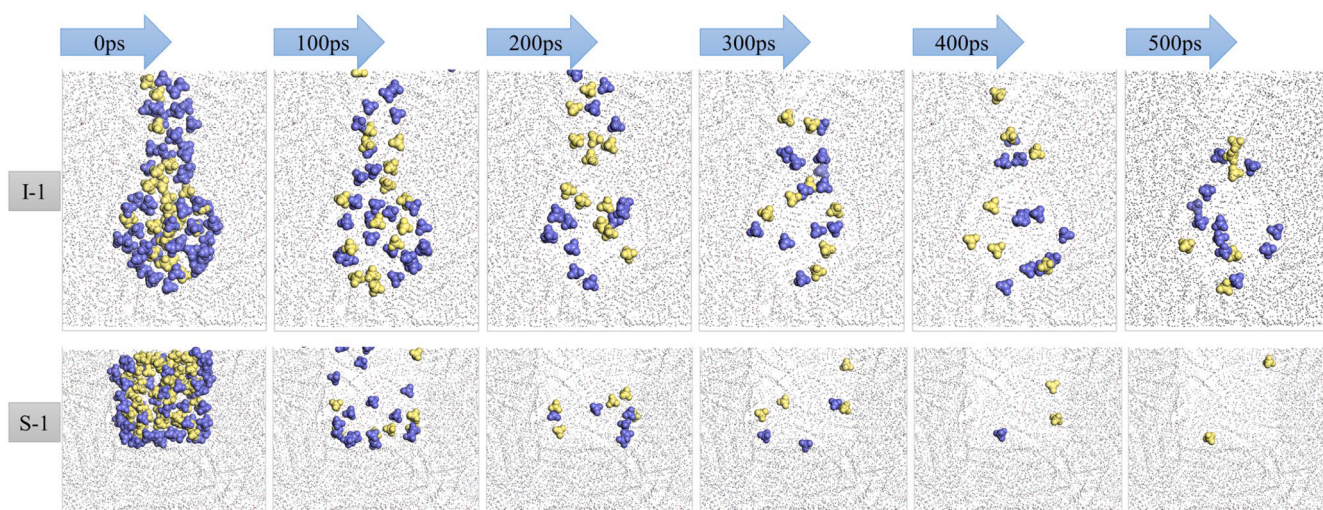


Fig. 11. Macroscopic desorption processes of CH₄ in the Ink-1 and Slit-1 pore models

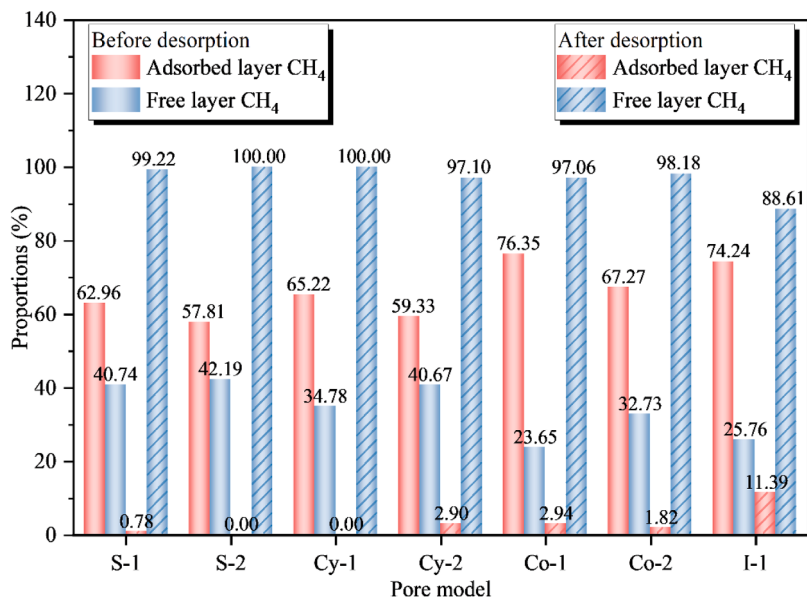


Fig. 12. Proportions of adsorbed-layer and free-layer CH_4 in D-pores and P-pores before and after desorption

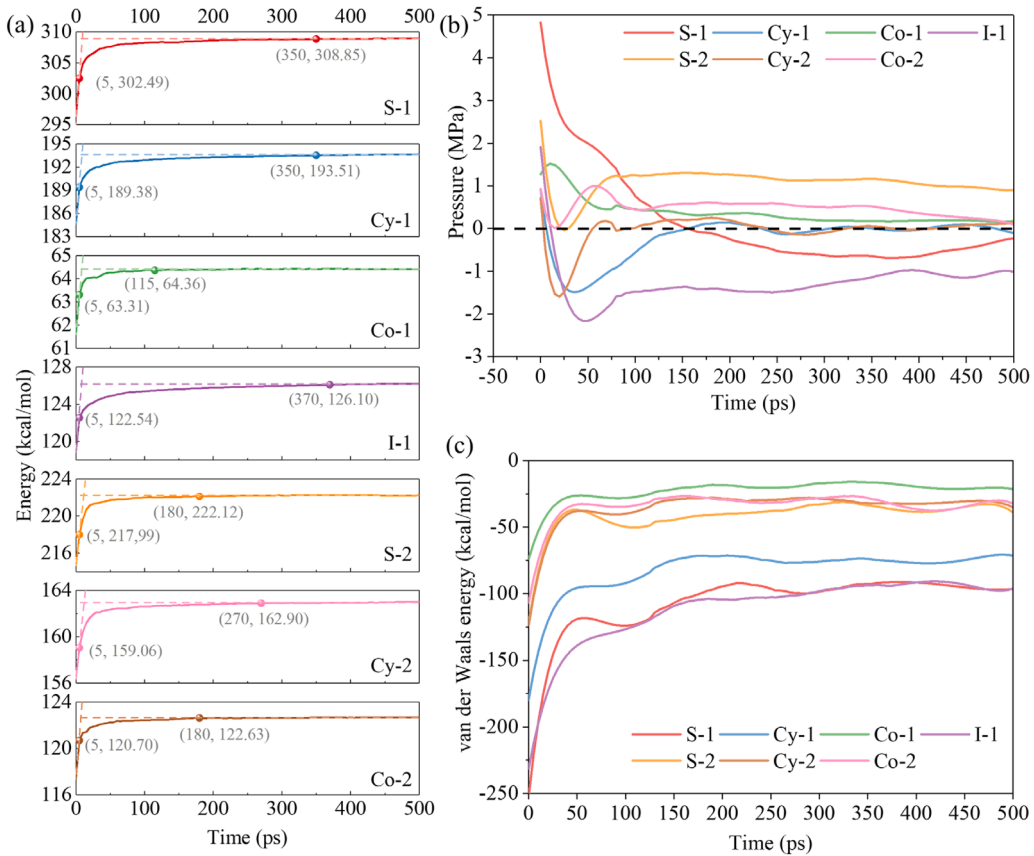


Fig. 13. Energy and pressure versus time curves during CH_4 desorption in different coal macromolecule pore models (a) Hamiltonian function; (b) System pressure; (c) van der Waals force

3.4. CH_4 diffusion characteristics in different morphological pore models

3.4.1. CH_4 diffusive characteristics

Fig. 14 shows the mean square displacement (MSD) and diffusion coefficient of the CH_4 desorption process in different pore models after MD simulation. It can be seen that in P-pores, the pore morphology has

less influence on the diffusion motion due to the physical structure of P-pores with openings at both ends. When the desorption motion starts, CH_4 molecules diffuse rapidly from the two sides of the channels to the outer low concentration in the gas-phase space. In D-pores, the difference in diffusion coefficients between different morphological pore models is as high as one order of magnitude, with the highest diffusion

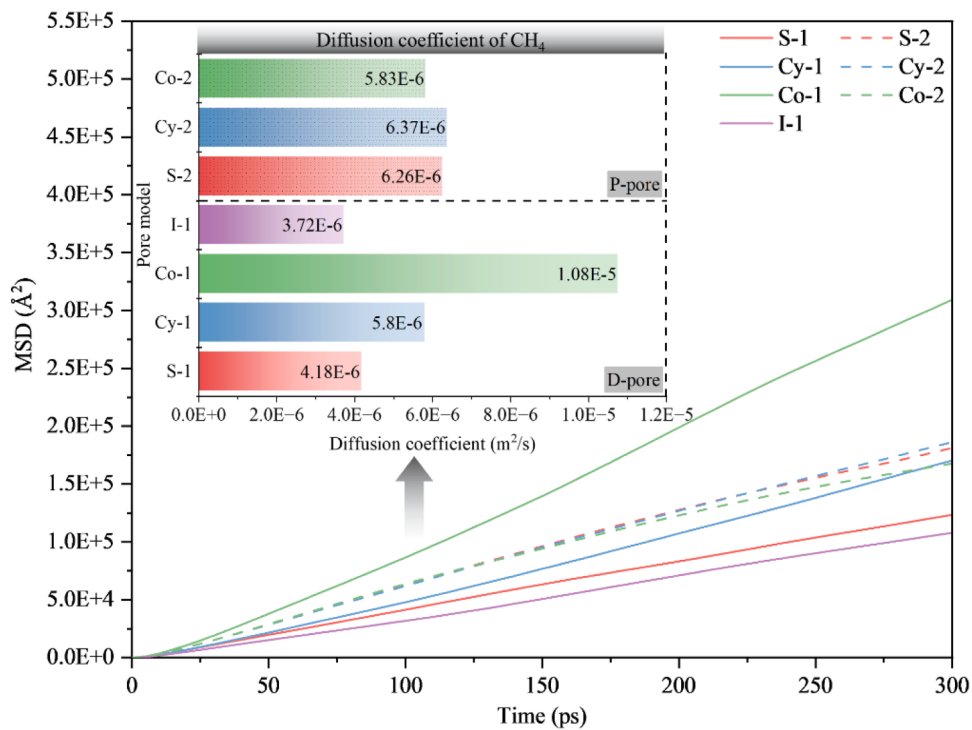


Fig. 14. MSD and diffusion coefficient of CH₄ during desorption in different pore models

coefficient for Co-1, the lowest for I-1, and the intermediate ones for Cy-1 and S-1. The reasons for this phenomenon are analysed as follows. Firstly, the structural characteristics of cone and ink bottle pores are opposite. Among others, the cone pore possesses an open space with a narrow inside and a vast outside, which provides a favourable spatial condition for the diffusion movement of CH₄ and promotes the diffusion movement of CH₄ molecules. In contrast, the ink bottle pore is a restricted space with a comprehensive inside and a narrow outside, and its narrow aperture restricts the diffusion of CH₄ molecules to the outside of the pore. Secondly, the gap in the number of CH₄ molecules within the pore space before desorption is significant, as shown in Fig. 4; the number of CH₄ molecules contained within I-1 is as much as two times that of Co-1. The greater the number of CH₄ molecules, the greater

the chance of molecular collision during diffusion movement. It has been shown that intermolecular collisions will both change the direction of motion and the magnitude of the speed of the molecules, as well as hinder the diffusion of the molecules to a certain extent, because the collisions will cause the kinetic energy of the molecules to be partially converted into other forms of energy, thus reducing the average kinetic energy of the molecules and the speed of diffusion. As a result, the diffusion motion of the CH₄ molecules in I-1 is relatively restricted.

3.4.2. Interaction strength

The radial distribution function (RDF) and coordination numbers (CN) of C atoms and CH₄ molecules in the pore models can characterise the possibility of CH₄ molecules appearing in a specific r range around

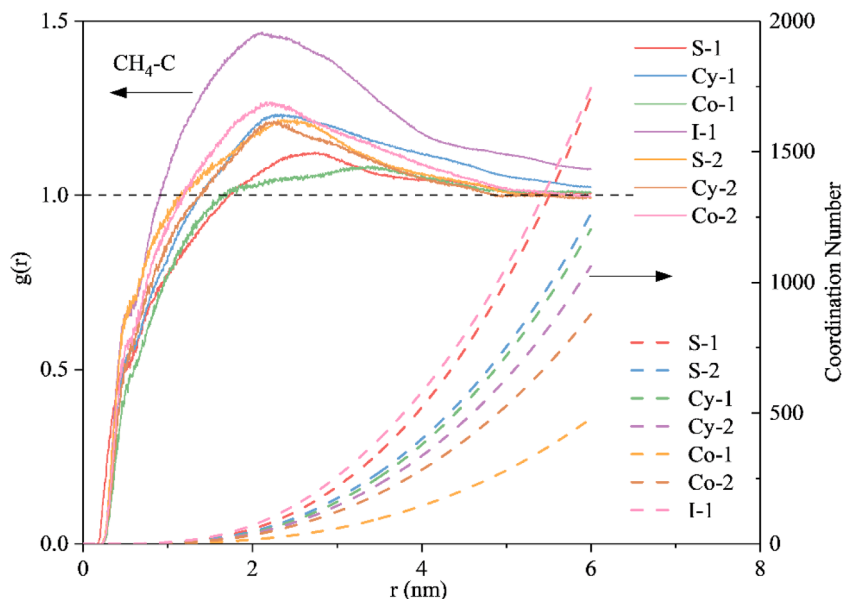


Fig. 15. RDF and CN curves of C atoms and CH₄ molecules in the different pore models

the coal molecules and the change of CH₄-C interaction strength during the desorption of CH₄ molecules into the gas-phase space process. As shown in Fig. 15, the first RDF peak of C-CH₄ in pore models appears at a distance r of 2–3.5 nm, indicating that CH₄ interacts most strongly with the C atoms in the coal molecule within the range and has the highest probability of appearing CH₄ molecules. When the distance is extended to about 5 nm, the value of $g(r)$ tends to be 1, which indicates that the CH₄-C interaction gradually weakened. However, ink bottles and cylinder C-pores require a much longer diffusion distance to achieve the above goal, and their desorption process under the same conditions is more complicated. Although each pore model possesses the same gas-phase space, the likelihood and number of CH₄ molecules appearing at the molecular distance where CH₄-C interactions are the strongest varies depending on the shape of the pores, with the possibilities being in the following order: I-1>Co-2>Cy-1>S-2>Cy-2>S-1>Co-1, which likewise confirms that CH₄-C interactions are the strongest and the most difficult to desorb in the ink bottle pore. Overall, the strength of CH₄-C interactions was much higher in D-pores than in P-pores.

3.5. Mechanism of microscopic influence of coals pore morphology on CH₄ adsorption-desorption-diffusion characteristics

Currently, it is difficult for experimental methods to reveal the influence of pore shape on the adsorption, storage and flow patterns of CBM. Therefore, molecular simulation methods have been widely used to study the gas storage and transport laws within the nanoscale pores of coal seams [41]. From the previous simulation results, under the same pore size conditions, there are significant differences in the CH₄ adsorption capacity and storage state in individual pores with different shapes or degrees of openness. The degree of pore openness is positively correlated with the amount of CH₄ molecules accommodated within the pore but negatively correlated with the pore surface coverage and surface adsorption capacity. The slit pores show obvious storage advantages among many pore structures. However, the analysis, in conjunction with the excess adsorption curves, reveals that the proportion of CH₄ in the adsorbed layer within the slit pores is lower than that of the other pore structures. In contrast, the amount of CH₄ in the free layer is on the high side. This means that the pore shape distribution trend and the degree of pore connectivity of the experimental coal samples can be roughly estimated to a certain extent based on the trend of the excess adsorption curves obtained from laboratory measurements. This is discussed by researchers such as Yin [23] and Song [37] in their studies on the adsorption and flow characteristics of CBM and shale gas, respectively.

For the desorption phenomenon, the gas desorption behaviour in the pores of organic matter has been defined by researchers as ‘micro-desorption’ and ‘macro-desorption’ from different perspectives [38]. The former studies the release of individual adsorbent particles from the adsorbent surface and corresponds to the desorption phenomenon during dynamic equilibrium in Section 3.1. The latter is the phenomenon of reduction of the total amount of adsorbed substances in the adsorbent under external conditions such as pressure or concentration, which corresponds to the desorption of gases from inside the coal pores into the gas-phase space outside the pores in Section 3.3, which is a common desorption phenomenon in practical engineering applications. Macro-desorption is usually completed very quickly, with most of the energy released in the early desorption stage, and a minimal amount of the remaining CH₄ gas will be released slowly in the later stage [42]. Still, they have not yet revealed the influence of the pore morphology on the abovementioned desorption phenomenon from the microscopic molecular point of view. Therefore, in this paper, the external gas-phase space was added based on the adsorption equilibrium configuration to simulate the macroscopic desorption phenomenon of CH₄ driven by the concentration gradient. New insights into the phenomenon of rapid desorption of coal gas were provided from the perspective of pore morphology.

In other words, when desorption occurs, gas molecules are generally the first to be desorbed from the pore surface and then diffusively transported through the pores in the matrix driven by the gas concentration. Therefore, this paper explains the limiting or driving effect of pore morphology on CH₄ desorption during the desorption process from the perspective of diffusion motion. As shown in Fig. 14, the diffusion coefficient of CH₄ molecules in I-1 is the smallest, and the diffusion motion is relatively restricted. From the results of RDF curves, it is also clear that the interaction between CH₄ molecules and C atoms in the pore wall in I-1 is the strongest, influenced by the pore shape. Therefore, when gas extraction is carried out if the coal seam contains many ink-bottle pores, a large amount of gas will be left in the coal seam. It is necessary to take effective treatment and protection measures in advance to avoid the storage phenomenon caused by the high gas content in the coal, to improve the efficiency of gas extraction, and at the same time, to reduce the risk of coal gas protrusion accidents.

Insufficiently, the main finding of this paper is that different morphological pore models present other adsorption properties and flow and transport laws, but the process of CH₄ gas escape and release inside the coals after the destruction of C-pores by disturbing stress has yet to be discussed. This is crucial for studying the structural evolution of coals under mining stress disturbance and the CH₄ transport process.

4. Conclusions

In this paper, considering the synergistic effect of pore shape and degree of openness on the storage and transport characteristics of CBM, different shapes of non-homogeneous coal bed pore structure models were constructed, and molecular simulation studies of CH₄ adsorption-desorption-diffusion were carried out in these pore models based on the GCMC-MD method. The changes in the characteristic laws of gas adsorption-desorption capacity, gas fugacity, diffusion coefficient and energy distribution with the pore shape and degree of openness were analysed to determine the influence of surface diffusion of adsorbed gas on gas transport. The results reveal the impact of the differences in pore morphology characteristics of coal beds on the storage and transport properties of CBM from a molecular point of view. Reliable research conclusions are provided for the efficient utilisation of CBM and the development of development technology. The findings of this study are as follows:

- (1) The saturation adsorption capacity of slit-shaped pores and P-pores is the highest, and the potential of CBM storage is the largest. The saturation adsorption pressure of C-pores and D-pores is lower than that of P-pores, but the adsorption potential energy and adsorption sites of C-pores and D-pores are higher than that of P-pores. The pore shapes have a lesser effect on the adsorption potential energy than the degree of pore openness. The pore openness was positively correlated with the gas storage capacity and negatively correlated with the adsorption potential energy.
- (2) Comparison of adsorbed-layer CH₄ amounts shows that those in slit, cylinder and ink bottle pores are higher than those in other pores, with those in slit pores being 1.5–3 times higher than those in other pores; the differences in C-pores and D-pores are more minor, but both are lower than those in P-pores, which is affected by the difference in SSA of pore models. Comparison of adsorbed-layer CH₄ proportions shows that cone pores >ink bottle pores >cylinder pores >sphere pores >slit pores; P-pores >D-pores >C-pores, which is the combined effect of pore model SSA and PV.
- (3) The effective flow diameters/widths of free-layer CH₄ within the different morphology pore models were calculated to be only 29.20%–74.50% of the actual pore diameters, so the effect of adsorbed-layer CH₄ thickness on the flow of free-layer CH₄ cannot be neglected. Except for the sphere and ink bottle pores,

- the K_n of free-layer CH₄ decreases with the increase of pore openness, while D_{K_n} shows an opposite trend.
- (4) almost all CH₄ molecules in the pore models except I-1 were desorbed during the macroscopic desorption simulation. Among others, the pore morphology has less influence on the diffusion movement of CH₄ in P-pores, which possess the physical structure of opening at both ends. The difference in diffusion coefficients between pore models of different morphologies can be as high as one order of magnitude, unlike that of the D-pores. The self-structured features of the Co-1 and I-1 pores promote and inhibit the diffusion behaviours of CH₄ desorption, respectively.
- (5) The interaction of the CH₄-C is the strongest in the 2–3.5 nm range around the coal molecules, with the highest probability of CH₄ molecules appearing. The CH₄ desorption process typically releases up to 97% of the total energy at 5ps and reaches its maximum within 50 to 370 ps. The energy values released by desorption are in the order of slit pore>cylinder pore> ink bottle pore>cone pore. The cone pores have the fastest desorption rate and the highest degree of energy jump, reaching the energy maximum first.

In the future, this paper's research method can be combined with fluid intrusion technology and scanning imaging technology to form a multi-scale coal reservoir pore structure characterisation method while validating its results. A bridge between microscopic molecules and macroscopic structures can be built to accurately predict the storage capacity and flow characteristics of CBM under different reservoir conditions, thus preventing coal and gas outbursts and improving the efficiency of CBM utilisation.

CRediT authorship contribution statement

Chao Xu: Writing – review & editing, Funding acquisition, Conceptualization, Supervision. **Wenjing Wang:** Writing – original draft, Methodology, Data curation, Funding acquisition. **Kai Wang:** Writing – review & editing, Funding acquisition, Supervision. **Lin Guo:** Data curation, Software, Writing – original draft. **Tong Yang:** Validation, Data curation, Writing – original draft. **Yongwang Yuan:** Investigation, Data curation, Software. **Yuanyuan Hu:** Investigation, Formal analysis.

Declaration of competing interest

The authors declare that we have no conflicts of interest.

Acknowledgements

This research is financially supported by the National Natural Science Foundation of China (52374251, 52130409 and 52121003) and the Fundamental Research Funds for the Central Universities (2023JCCXAQ03 and Ph.D. Top Innovative Talents Fund of CUMTB).

Data availability

Data will be made available on request.

References

- [1] L. Qi, X. Tang, Z. Wang, X. Peng, Pore characterization of different types of coal from coal and gas outburst disaster sites using low temperature nitrogen adsorption approach, *Int. J. Min. Sci. Technol.* 27 (2) (2017) 371–377.
- [2] J. Wei, H. Liu, X. Xu, Y. Liu, P. Xie, Y. Gao, Analysis of damage characteristics and influencing factors of coal cut by cutting tooth based on industrial CT technology, *Process Safety Environ. Protec.* 184 (2024) 936–949.
- [3] K. Zeng, P. Jiang, R. Xu, Restricted CO₂/CH₄ diffusion in nanopores: a quantitative framework to characterize nanoconfinement effect of shale organic pore, *Int. J. Heat. Mass Transf.* 210 (2023) 124178.
- [4] C. Xu, L. Qin, K. Wang, H. Sun, M. Cao, Gas seepage laws based on dual porosity and dual permeability: numerical simulation and coalbed methane extraction practice, *Energy Sci. Eng.* 9 (4) (2021) 509–519.
- [5] X. Wang, Y. Cheng, D. Zhang, H. Yang, X. Zhou, Z. Jiang, Experimental study on methane adsorption and time-dependent dynamic diffusion coefficient of intact and tectonic coals: implications for CO₂-enhanced coalbed methane projects, *Process Safety Environ. Protec.* 156 (2021) 568–580.
- [6] H. Yang, W. Bi, Y. Zhang, J. Yu, J. Yan, D. Lei, Z. Ma, Effect of tectonic coal structure on methane adsorption, *J. Environ. Chem. Eng.* 9 (6) (2021) 106294.
- [7] C. Yang, J. Zhang, S. Han, X. Wang, L. Wang, W. Yu, Z. Wang, Compositional controls on pore-size distribution by nitrogen adsorption technique in the Lower Permian Shanxi Shales, Ordos Basin, *J. Nat. Gas. Sci. Eng.* 34 (2016) 1369–1381.
- [8] Y. Zhang, D. Li, G. Xin, S. Ren, A review of molecular models for gas adsorption in shale nanopores and experimental characterization of shale properties, *ACS Omega* 8 (15) (2023) 13519–13538.
- [9] S. Barbhuiya, B.B. Das, Molecular dynamics simulation in concrete research: a systematic review of techniques, models and future directions, *J. Build. Engineer.* 76 (2023) 107267.
- [10] M. Thommes, K. Kaneko, A.V. Neimark, J.P. Olivier, F. Rodriguez-Reinoso, J. Rouquerol, K.S.W. Sing, Physisorption of gases, with special reference to the evaluation of surface area and pore size distribution (IUPAC Technical Report), *Pure Appl. Chem.* 87 (9–10) (2015) 1051–1069.
- [11] Z. Li, D. Liu, Y. Cai, Y. Wang, J. Teng, Adsorption pore structure and its fractal characteristics of coals by N₂ adsorption/desorption and FESEM image analyses, *Fuel* 257 (2019) 116031.
- [12] B. Nie, X. Liu, L. Yang, J. Meng, X. Li, Pore structure characterization of different rank coals using gas adsorption and scanning electron microscopy, *Fuel* 158 (2015) 908–917.
- [13] L. Si, Z. Li, M. Kizil, Z. Chen, Y. Yang, S. Ji, The influence of closed pores on the gas transport and its application in coal mine gas extraction, *Fuel* 254 (2019) 115605.
- [14] K. Wang, Multiscale characteristics of pore-fracture structures in coal reservoirs and their influence on coalbed methane (CBM) transport: a review, *Geener. Sci. Engineer.* 242 (2024) 213181.
- [15] J. Li, Y. Wang, Z. Chen, S.S. Rahman, Simulation of adsorption–desorption behavior in coal seam gas reservoirs at the molecular level: a comprehensive review, *Energy Fuels* 34 (3) (2020) 2619–2642.
- [16] Y. Song, B. Jiang, C. Wei, X. Dai, F. Quan, C. Hou, G. Cheng, A review on the application of molecular dynamics to the study of coalbed methane geology, *Front. Earth. Sci. (Lausanne)* 9 (2021) 775497.
- [17] W. Zhou, J. Zhu, H. Wang, D. Kong, Transport diffusion behaviors and mechanisms of CO₂/CH₄ in shale nanopores: insights from molecular dynamics simulations, 36 (19) (2022) 11903–11912.
- [18] K. Wang, S. Lin, W. Zhao, Reviews on simulation studies of coalbed gas recovery and transport processes, *Energy Fuels* 37 (19) (2023) 14622–14644.
- [19] A. Sidorenkov, M. Stukan, V. Ivanov, Methane flow in nanopores: analytical approximation based on MD simulations, *Fuel* 332 (2023).
- [20] Y. Shi, Y. Liu, J. Xue, S. Li, C. Zhang, Study on methane adsorption/desorption and flow law in the nanopores of coal based on LAMMPS, *Coal Geol. Explor.* 51 (2023) 37–45.
- [21] M. Hao, C. Wei, H. Zhang, Adsorption and diffusion of methane in coal slit pores: insights into the molecular level, *Energy Fuels* 36 (2) (2022) 880–886.
- [22] L. Chen, D. Huang, S. Wang, Y. Nie, Y. He, W. Tao, A study on dynamic desorption process of methane in slits, *Energy* 175 (2019) 1174–1180.
- [23] T. Yin, D. Liu, Y. Cai, Z. Liu, M. Gutierrez, A new constructed macromolecule-pore structure of anthracite and its related gas adsorption: a molecular simulation study, *Int. J. Coal. Geol.* 220 (C) (2020) 103415.
- [24] J. Meng, S. Zhang, Z. Cao, C. Wang, Insight on coal molecular-scale pore reconstruction of Tunliu mine and its characterization and analysis, *J. China Coal Soc.* 47 (2022) 160–170.
- [25] M. Zhang, Z. Liu, B. Pan, S. Iglauer, Z. Jin, Molecular simulation on CO₂/H₂S co-adsorption in organic and inorganic shale nanopores, *Appl. Surf. Sci.* 624 (2023) 157167.
- [26] X. Liu, X. He, N. Qiu, X. Yang, Z. Tian, M. Li, Y. Xue, Molecular simulation of CH₄, CO₂, H₂O and N₂ molecules adsorption on heterogeneous surface models of coal, *Appl. Surf. Sci.* 389 (2016) 894–905.
- [27] Y. Dang, L. Zhao, X. Lu, J. Xu, P. Sang, S. Guo, H. Zhu, W. Guo, Molecular simulation of CO₂/CH₄ adsorption in brown coal: effect of oxygen-, nitrogen-, and sulfur-containing functional groups, *Appl. Surf. Sci.* 423 (2017) 33–42.
- [28] M. Yuan, W. Nie, W. Zhou, J. Yan, Q. Bao, C. Guo, P. Tong, H. Zhang, L. Guo, Determining the effect of the non-ionic surfactant AEO₉ on lignite adsorption and wetting via molecular dynamics (MD) simulation and experiment comparisons, *Fuel* 278 (2020).
- [29] C. Xu, W. Wang, K. Wang, A. Zhou, L. Guo, T. Yang, Filling-adsorption mechanism and diffusive transport characteristics of N₂/CO₂ in coal: experiment and molecular simulation, *Energy* 282 (2023) 128428.
- [30] Q. Zhang, H. Zhu, R. Kang, L. Zhang, S. Fang, L. Hu, B. Qu, Q. Liao, Insight into the effect of biaxial compression strain on adsorption structure of bituminous coal matrix as well as gas diffusion and permeability properties by macromolecule simulation, *Fuel* 338 (2023).
- [31] B. Hu, Y. Cheng, Z. Pan, Classification methods of pore structures in coal: a review and new insight, *Gas Sci. Engineer.* 110 (2023) 204876.
- [32] H. Liu, J. Liu, D. Gao, Z. Fan, H. Xu, H. Ding, H. Fang, K. Zhang, New insight into CH₄ adsorption mechanism in coal based on modeling analysis of different adsorption theories, *J. Environ. Chem. Eng.* 12 (4) (2024) 113174.

- [33] Z. Yang, Z. Yin, W. Xue, Z. Meng, Y. Li, J. Long, J. Wang, Construction of Buertai coal macromolecular model and GCMC simulation of methane adsorption in micropores, *ACS. Omega* 6 (17) (2021) 11173–11182.
- [34] S. Deng, X. Li, B. Xu, Modeling dynamic gas desorption in coal reservoir rehabilitation: molecular simulation and neural network approach, *ACS. Omega* 7 (50) (2022) 46051–46065.
- [35] Z. Wang, Y. Cheng, L. Wang, H. Zhou, X. He, M. Yi, C. Xi, Characterization of pore structure and the gas diffusion properties of tectonic and intact coal: implications for lost gas calculation, *Process Safety Environ. Protec.* 135 (C) (2020) 12–21.
- [36] W. Zhao, Y. Cheng, Z. Pan, K. Wang, S. Liu, Gas diffusion in coal particles: a review of mathematical models and their applications, *Fuel* 252 (2019) 77–100.
- [37] W. Song, J. Yao, K. Zhang, Study on gas adsorption and transport behavior in shale organic nanopore, *Chin. J. Theoret. Appl. Mech.* 53 (2021) 2179–2192.
- [38] M. Pillalamarry, S. Harpalani, S. Liu, Gas diffusion behavior of coal and its impact on production from coalbed methane reservoirs, *Int. J. Coal. Geol.* 86 (4) (2011) 342–348.
- [39] Y. Zeng, Z. Ning, Q. Wang, H. Sun, L. Huang, H. Ye, Gas transport in self-affine rough microchannels of shale gas reservoir, *J. Petrol. Sci. Engineer.* 167 (2018) 716–728.
- [40] Z. Li, T. Ren, X. Li, Y. Cheng, X. He, J. Lin, M. Qiao, X. Yang, Full-scale pore structure characterization of different rank coals and its impact on gas adsorption capacity: a theoretical model and experimental study, *Energy* 277 (2023) 127621.
- [41] Y. Song, Y. Zhu, L. Wu, Macromolecule simulation and CH₄ adsorption mechanism of coal vitrinite, *Appl. Surf. Sci.* 396 (2017) 291–302.
- [42] Q. Zou, B. Lin, T. Liu, X. Hu, C. Zheng, Variations in coalbed gas content, initial gas desorption property and coal strength after drilling-slotting integration technique and gas drainage: insight into pore characteristics, *Int. J. Oil Gas Coal Technol.* 15 (3) (2017) 235–266.